Integrated modeling, finite-element analysis, and engineering design for thin-shell structures using subdivision

Article *in* Computer-Aided Design · February 2002

DOI: 10.1016/S0010-4485(01)00061-6 · Source: DBLP

5 authors, including:

Michael J. Scott
University of Illinois at Chicago
49 PUBLICATIONS **918** CITATIONS

SEE PROFILE

Erik Antonsson
California Institute of Technology
107 PUBLICATIONS **2,439** CITATIONS

SEE PROFILE

Peter Schröder
California Institute of Technology
211 PUBLICATIONS **10,454** CITATIONS

SEE PROFILE

Integrated Modeling, Finite-Element Analysis, and Engineering Design for Thin-Shell Structures using Subdivision

Fehmi Cirak, Michael J. Scott,
Erik K. Antonsson, Michael Ortiz, Peter Schröder

Division of Engineering and Applied Science
California Institute of Technology
Pasadena, CA 91125, U.S.A.

Abstract

Many engineering design applications require geometric modeling and mechanical simulation of thin flexible structures, such as those found in the automotive and aerospace industries. Traditionally, geometric modeling, mechanical simulation, and engineering design are treated as separate modules requiring different methods and representations. Due to the incompatibility of the involved representations the transition from geometric modeling to mechanical simulation, as well as in the opposite direction, requires substantial effort. However, for engineering design purposes efficient transition between geometric modeling and mechanical simulation is essential. We propose the use of subdivision surfaces as a common foundation for modeling, simulation, and design in a unified framework. Subdivision surfaces provide a flexible and efficient tool for arbitrary topology free-form surface modeling, avoiding many of the problems inherent in traditional spline patch based approaches. The underlying basis functions are also ideally suited for a finite element treatment of the so-called thin shell equations, which describe the mechanical behavior of the modeled structures. The resulting solvers are highly scalable, providing an efficient computational foundation for design exploration and optimization. We demonstrate our claims with several design examples, showing the versatility and high accuracy of the proposed method.

1 Introduction

Current engineering design practice in industry employs a sequence of tools which are generally not well matched to each other. For example, the output of a computer aided geometric design (CAGD) system is typically not suitable as direct input for a finite-element modeler. This is usually addressed through intermediate tools such as mesh generators. Unfortunately these are notoriously lacking in robustness. Even once a geometric model has been successfully meshed, the output of a finite-element simulation cannot be directly applied to the original geometric model, since there is no straightforward mapping back to the original design degrees of freedom. Additionally there is a need for a trade-off between the speed of analysis and the fidelity of the results. In the early stages of design, quick results are necessary, but approximate results are acceptable. In the the later stages, highly precise results are required, and with longer computation times tolerated. Worse, different underlying models are required for each level of refinement. These difficulties make the design process cumbersome and inhibit multiple, rapid iteration on different design choices. Many of these difficulties can be greatly reduced in a unified representation paradigm, *e.g.*, an environment in which the geometric model uses the same underlying representation as the appropriate finite-element simulation. The principal advantage of such a unified representation paradigm is the simple and rapid data transfer between the geometric design and finite-element analysis tools. No cumbersome remodeling of already generated geometric models for purposes of finite-element simulation is required. As a result the investigation of different design alternatives, *e.g.*, for design space exploration, will be substantially simplified. In applications this will lead to faster product development cycles through the tight combination of the design and analysis steps.

Historically modeling and simulation tools were developed in different communities with limited interactions. To our knowledge few attempts have been made in the past to unify geometric modeling and simulation based on a common representation paradigm [17, 20]. Our contribution in this paper is a computationally simple and theoretically well-justified framework for free-form geometric modeling coupled with finite-element analysis of thin-shells for purposes of engineering design. Thin flexible structures (plates and shells) appear in many areas of applied engineering design, *e.g.*, in automobile and aerospace industries. As the underlying representation we have chosen subdivision surfaces. They have many advantages for free form geometric modeling in particular for shapes of arbitrary topology. With the recent development of subdivision algorithms supporting such important modeling operations as trimming, boundary interpolation, or description of small features [5, 19, 23, 24], subdivision surfaces are well positioned to become important a fundamental modeling primitive for CAGD applications [2]. At the same time it has been demonstrated recently [10] that subdivision basis functions can serve as shape functions in the context of finite-element thin-shell analysis, with excellent performance and accuracy. Similar to a thin-*plate*, the deformation of curved *shells* is described by partial differential equations with derivatives up to order four, requiring shape functions with square integrable curvatures for finite-element treatments. The choice of subdivision shape functions can be contrasted with more traditional approaches for the construction of shape functions, which are typically based on Hermite interpolation. It is well known that this leads to fifth order polynomials over triangles [50]. Higher order shape functions however are not suitable for practical problems with *e.g.* reentrant corners, jumps in the material properties, or point loads which exhibit singularities in the exact solution. Subdivision surfaces satisfy the necessary analytic requirements while being parameterized strictly in terms of displacements only and circumvent the usual difficulties with traditional finite-element treatments.

The many advantages of the subdivision method for geometric modeling *and* for mechanical simulation makes it a method of choice for integrated design and simulation. The need to convert an existing CAD model to a finite-element mesh and the difficulty of doing so robustly is entirely circumvented. Since the finite-element solver uses the same degrees of freedom as the free-form geometric modeling system, optimization of the geometry based on the results of mechanics simulations is immediate. The latter in particular greatly facilitates the iterative process of engineering design.

1.1 Overview

In Section 2 we briefly review subdivision surfaces. In the present paper we restrict our framework to Loop surfaces [25] which generalize classic quartic box-splines, but we hasten to point out that the basic algorithms are equally applicable to other subdivision schemes, in particular the scheme of Catmull and Clark [8] which generalizes bi-cubic splines. Both subdivision schemes have the necessary smoothness to be ideally suited as shape functions in the finite-element treatment of thin-shell equations. Section 3 describes the formulation of equations governing the mechanical behavior of thin flexible structures. Finally, Section 4 discusses a basic framework for design space exploration and presents an integrated framework for modeling, simulation and design with subdivision surfaces. Two engineering design examples (square plate and car hood) are used to demonstrate the proposed approach.

2 Brief Review of Subdivision Surfaces

Subdivision schemes construct smooth surfaces through a limiting procedure of repeated refinement starting from an initial control mesh. In this sense they behave very much like knot doubling approaches applied to a spline surface control mesh. Generally, subdivision schemes consist of two steps. First the mesh is refined, *i.e.*, by quadrisection of all faces. Second, new nodal positions are computed for all vertices. These positions are simple, linear combinations of the nodal positions of the coarser mesh. For the schemes, of interest these computations are local, *i.e.*, they involve only nodal positions of the coarser mesh within a small, finite topological neighborhood, leading to efficient implementations. Using a suitable choice of weights, such subdivision schemes can be designed to produce a smooth surface in the limit [35, 51]. Subdivision methods which result in limit surfaces whose curvature tensor is square integrable are especially appealing for geometric modeling applications and purposes of thin-shell analysis.

The first subdivision schemes were proposed by Catmull and Clark [8] and Doo and Sabin [11] to address a shortcoming of traditional spline patches when modeling arbitrary topology surfaces. When assembling complex shapes out of spline patches, the Euler characteristic of the control mesh implies that "irregular vertices" cannot be avoided in the general case. For quadrilateral patches, these are control vertices where other than four patches meet; while for triangular patches, irregular vertices are those of valence other than six. At irregular vertices, cross patch continuity conditions can in general not be maintained. Catmull and Clark as well as Doo and Sabin proposed to address this challenge by generalizing the knot doubling rules associated with bi-cubic, respectively bi-quadratic splines around irregular vertices. The result are arbitrary topology smooth surfaces which consist of spline patches almost everywhere and are globally smooth for almost all initial control point configurations.

Many other schemes have been proposed and studied extensively in the mathematical geometric modeling literature (for an overview the interested reader is referred to [52]). All methods can be classified according to a small number of criteria. They can be interpolating or approximating, use triangular or quadrilateral patches, or be based on splitting either faces (primal schemes) or vertices (dual schemes). For example the scheme of Catmull and Clark is primal, based on quadrilaterals and is approximating, while the scheme of Doo and Sabin is dual, uses quadrilaterals, and is approximating. Interpolating primal schemes based on triangles were introduced by Dyn *et al*. [12] and improved by Zorin *et al*. [53], while Kobbelt, *et al*., [20] constructed a quadrilateral interpolating scheme. These latter schemes are generally not smooth enough for either geometric modeling or finite-element analysis of thin-shells.

For our purposes we have chosen the triangle-based primal approximating scheme of Loop [25]. It generalizes the knot doubling rules of quartic box splines to the arbitrary topology setting and yields globally C^2 surfaces except at irregular vertices where the surfaces are only C^1. While the curvatures at these points diverge, the curvatures are square integrable [36] as required for thin-shell analysis.

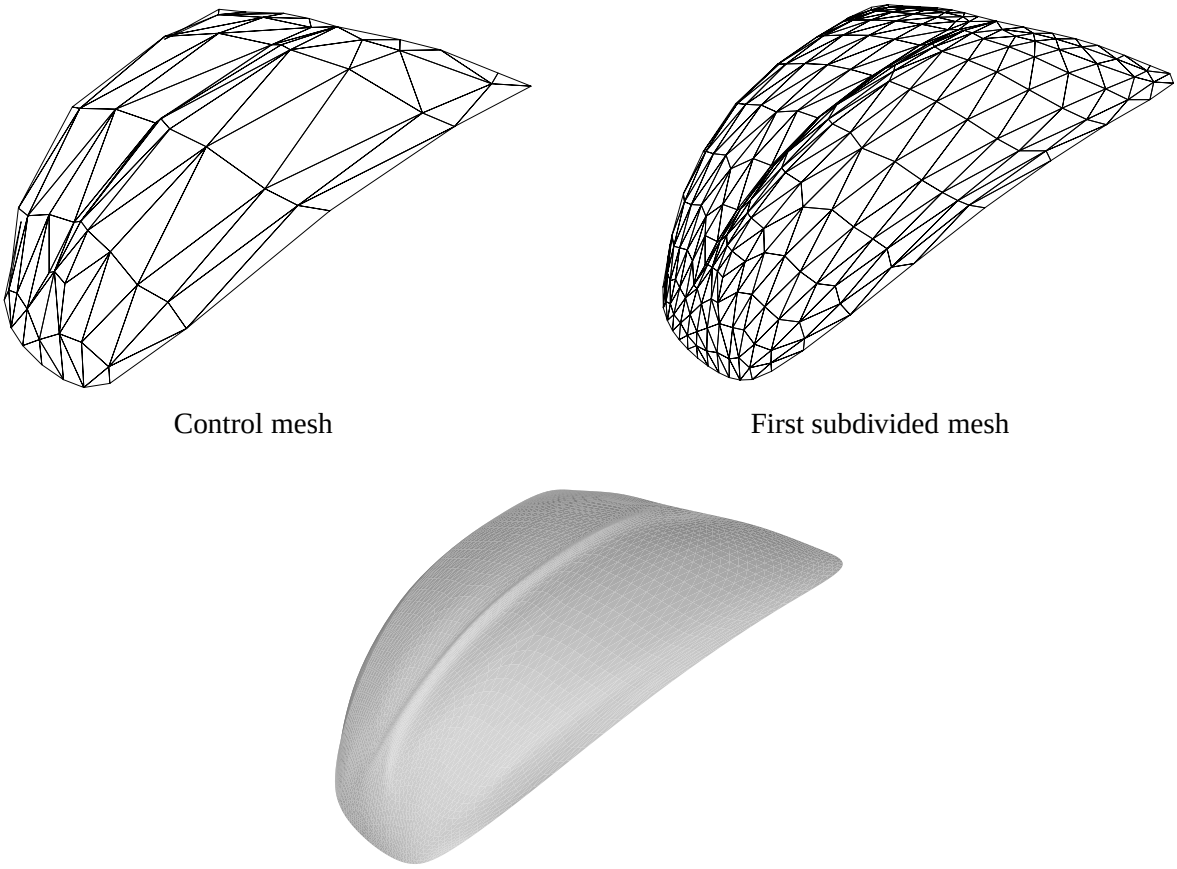

Control mesh First subdivided mesh

Limit surface

Figure 1: Loop's scheme.

In the following sections we state the refinement rules used in Loop's subdivision scheme for surfaces. While we focus on Loop's scheme, we hasten to point out that the basic ideas and machinery apply equally well to other subdivision schemes. In particular, the Catmull-Clark scheme, with quadrilateral elements, is a promising alternative for finite-element computations.

2.1 Loop's Scheme

In Loop's subdivision scheme, the control mesh and all refined meshes consist only of triangles. These are refined by quadrisection (Fig. 1 left side). The nodal positions of the new mesh are computed as local affine combinations of nearby nodal points in the coarser mesh. We distinguish two types of rules, those which compute newly inserted points (odd rules) and those which compute new nodal positions for vertices already present in the coarser mesh (even rules). Using the notation in Figure 2 odd points are computed as:

$$\boldsymbol{x}^{i+1}_{\text{odd}} = \frac{1}{8}(3\boldsymbol{x}^{i}_{\text{left}} + 3\boldsymbol{x}^{i}_{\text{right}} + \boldsymbol{x}^{i}_{\text{top}} + \boldsymbol{x}^{i}_{\text{bottom}})$$

while even points are updated as:

$$\boldsymbol{x}^{i+1}_{\text{center}} = (1 - kw)\boldsymbol{x}^{i}_{\text{center}} + w\sum_{l=1}^{k}\boldsymbol{x}^{i}_{l}$$

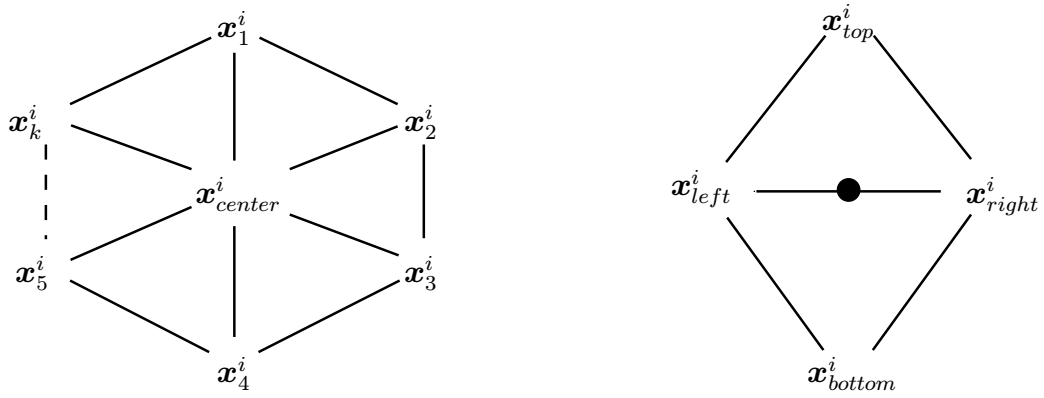

Figure 2: Refinement mask for Loop's subdivision scheme.

where $\boldsymbol{x}^i$ are the nodal positions of the mesh at level i and $\boldsymbol{x}^{i+1}$ are the nodal positions for the mesh $i+1$. The valence of a vertex, *i.e.*, the number of edges incident on it, is denoted by k. Note that all newly generated vertices have valence six while only the vertices of the original mesh may have valence other than six.

In the original scheme Loop [25] proposed weights:

$$w = \frac{1}{k}\left[\frac{5}{8} - \left(\frac{3}{8} + \frac{1}{4}\cos\frac{2\pi}{k}\right)^2\right]$$

Other values for w also give smooth surfaces. For example, Warren [48] proposed a simpler choice for w:

$$w = \frac{3}{8k} \quad \text{for} \quad k > 3 \quad \text{and} \qquad w = \frac{3}{16} \quad \text{for} \quad k = 3$$

Note that the weights used by the subdivision scheme depend only on the connectivity of the mesh and are independent of the nodal positions themselves. For the case $k = 6$ these rules reproduce the well known knot doubling rules for quartic box splines. As a consequence, the surface consists of quartic box spline patches everywhere except near the irregular vertices where it can be thought of as consisting of an infinite sequence of ever shrinking rings of quartic box spline patches.

So far we have ignored the boundary of the mesh, where the subdivision rules need to be modified. A very simple method applies the cubic spline knot doubling rules at the boundary. This method will produce cubic splines on the boundary if all boundary vertices are valence four. The presence of irregular vertices on the boundary as well as corners (concave as well as convex) requires different subdivision rules (see for example Biermann, *et al.*, [5]). In some applications it may be necessary to match boundary curves exactly which are not splines. Such transfinite interpolation can also be achieved through suitable modification of the rules near the boundary [24].

In any case, as we discuss below, evaluation of the necessary limit surface quantities can be achieved in a straightforward manner after only one or two subdivision steps (the exact number depends on the nature of the rules used [5]).

2.2 Limit Surface Evaluation

Even though subdivision surfaces are defined through a limit procedure, it is possible to evaluate the surface and its derivatives exactly at arbitrary parameter values based on eigen analysis of the subdivision operator [44, 43]. We are interested only in specific parameter values, namely those needed for quadrature

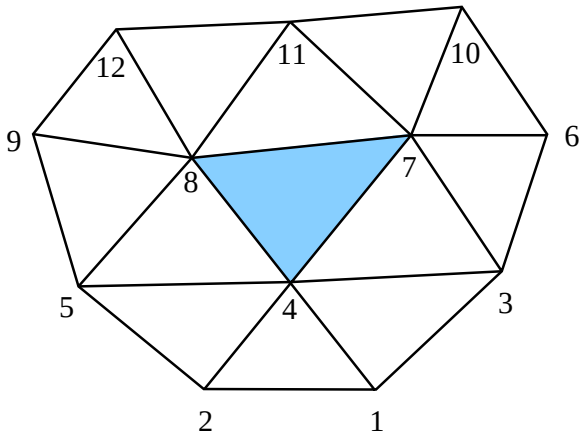

Figure 3: Quartic box spline patch.

evaluation of stiffness integrals arising from the computation of the mechanical response of the surface. For this the fully general method is not needed. In particular one-point quadratures are sufficient. These require the evaluation of positions and derivatives at the barycenter of an element.

A convenient local parameterization of the limit surface may be obtained as follows. For each triangle in the control mesh we choose (θ^1,θ^2) as two of its barycentric coordinates within their natural range:

$$T=\{(\theta^1,\theta^2),\ \text{s. t. } \theta^\alpha\in[0,1],\ 0\le\theta^1+\theta^2\le 1\}$$

The triangle T in the (θ^1,θ^2)-plane may be regarded as a master or standard element domain. It should be emphasized that this parameterization is defined locally for each element in the mesh. The entire discussion of parameterization and function evaluation may therefore be couched in local terms.

For regular patches, Loop's scheme leads to quartic box splines. Therefore, the local parameterization of the limit surface may be expressed in terms of box-spline shape functions, with the result:

$$\boldsymbol{x}(\theta^1,\theta^2)=\sum_{l=1}^{12}N^l(\theta^1,\theta^2)\boldsymbol{x}_l \tag{1}$$

where now the labels l refer to the local numbering of the nodes (see Figure 3). The precise form of the shape functions $N^l(\theta^1,\theta^2)$ is given in [10]. The embedding (eq. 1) may thus be regarded as a conventional isoparametric mapping from the standard domain T onto the limit surface Ω, with (θ^1,θ^2) playing the role of natural coordinates.

For function evaluation on irregular patches the mesh has to be subdivided until the parameter value of interest is interior to a regular patch. At that point the regular box spline parameterization applies once again. It should be noted that the refinement is performed for parameter evaluation only. For simplicity we assume that irregular patches have one irregular vertex only. This restriction can always be met for arbitrary initial meshes through one step of subdivision, which has the effect of separating all irregular vertices. As shown in Figure 4, after one subdivision step the triangles marked one, two, and three are regular patches. The action of the subdivision operator for this entire neighborhood can be described by a matrix:

$$\boldsymbol{X}^1=\boldsymbol{A}\boldsymbol{X}^0$$

The matrix $\boldsymbol{A}$ has dimension $(k+12,\ k+6)$ and its entries can be derived from the subdivision rules as presented in Section 2.1. For the proposed shell element with one point quadrature at the barycenter of the element, a single subdivision step is sufficient, since the sampling point (center of the initial patch) lies in

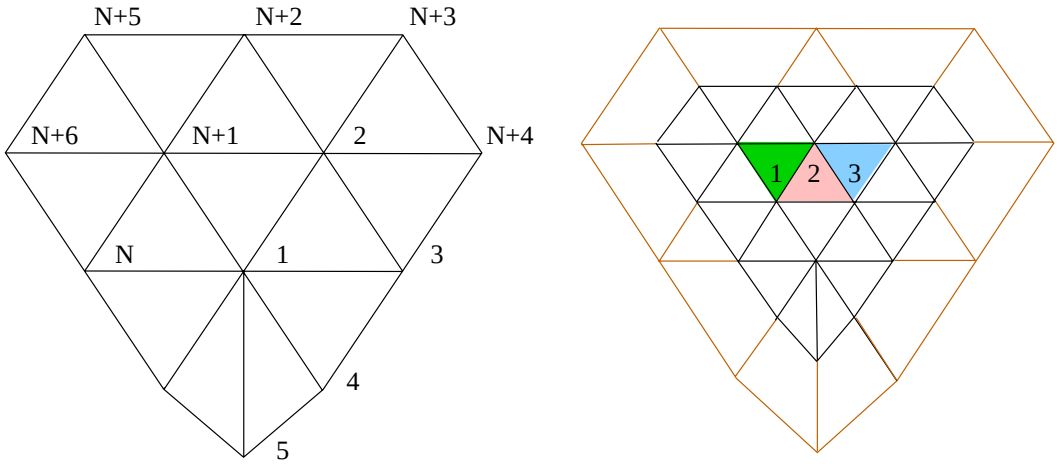

Figure 4: Refinement near an irregular vertex.

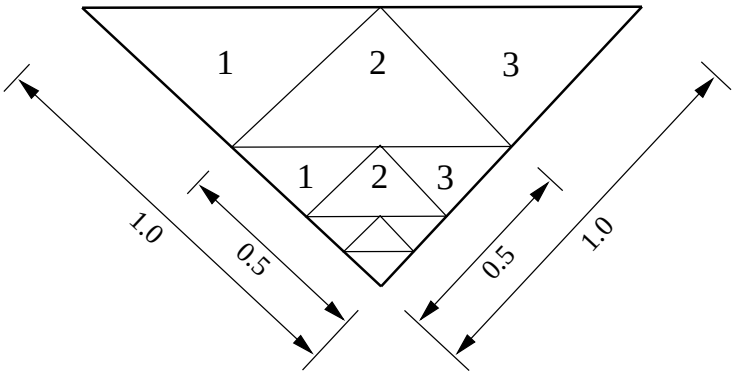

Figure 5: Refinement in the parameter space.

sub-patch 2. We define 12 selection vectors $\boldsymbol{P}_l$, $l = 1, \ldots, 12$ of dimension $(k + 12)$ which extract the 12 box-spline control points for sub-patch 2 from the $k + 12$ points of the refined mesh. The entries of $\boldsymbol{P}_l$ are zero and one depending on the indices of the initial and refined meshes. To evaluate the function values in the three triangles with the box-spline shape functions N^l, a coordinate transformation must be performed. The relation between the coordinates (θ^1, θ^2) of the original triangles and the coordinates $(\tilde{\theta}^1, \tilde{\theta}^2)$ of the refined triangles can be established from the refinement pattern in Figure 5. For the center of sub-patch 2 we have the following relation:

Triangle 2: $\quad \tilde{\theta}^1 = 1 - 2\theta^1 \qquad$ and $\quad \tilde{\theta}^2 = 1 - 2\theta^2$

The function values and derivatives for sub-patch 2 can now be evaluated using the interpolation rule:

$$\boldsymbol{x}(\theta^1, \theta^2) = \sum_{l=1}^{12} N^l(\tilde{\theta}^1, \tilde{\theta}^2) \boldsymbol{P}_l \boldsymbol{A} \boldsymbol{X}^0 \tag{2}$$

Derivatives, such as required for the computation of the potential energy, follow by direct differentiation of the interpolation rule (eq. 2).

3 Review of Thin-Shell Equations

The mechanical response of a subdivision surface with an attached thickness property can be computed with the classical Kirchhoff-Love shell theory. In this section we briefly summarize the resulting field equations. A detailed presentation of classical shell theories can be found in [29]. The final result of our derivation will be couched in terms of constrained energy minimization where the internal energy of the shell depends on *intrinsic* quantities of the surface such as the first and second fundamental form.

3.1 Related Methods in Geometric Modeling

Before going into the details of the description of the mechanical behavior of shells, it is useful to briefly contrast our approach with other energy minimization methods. These often appear in variational modeling. For example, Halstead, *et al.*, [14] described an algorithm for fair interpolation of a given set of points with a Catmull-Clark surface. To constrain the solution space they search for a parameterized surface $\boldsymbol{x}$ which simultaneously interpolates the given constraints and minimizes an energy functional Φ over the domain Ω based on a weighted average of squared first and second derivatives:

$$\Phi[\boldsymbol{x}] = \alpha \int_\Omega (\boldsymbol{x}_{,1})^2 + (\boldsymbol{x}_{,2})^2 d\Omega + \beta \int_\Omega (\boldsymbol{x}_{,11})^2 + 2(\boldsymbol{x}_{,12})^2 + (\boldsymbol{x}_{,22})^2 d\Omega$$

where α and β are some prescribed constants and a comma is used to denote partial differentiation. These terms are sometimes referred to as stretching and bending energies. While such formulations are typically derived from a thin-*plate* ansatz they cannot describe the *mechanical* behavior of a *shell* correctly since the result of the computation depends on the particular parameterization chosen. In fact using the standard parameterization (see Section 2.2) leads to infinite bending energies [14] and either zero or infinite stretching energies near irregular vertices. Such methods can nonetheless be useful for scattered data interpolation after suitable modifications near the extraordinary vertices [27] or elimination of the infinite energy modes [14]. To accurately and consistently describe the mechanical behavior of shells a formulation in terms of intrinsic surface properties is required.

3.2 Kinematics of Deformation

We begin by considering a shell whose undeformed geometry is characterized by a subdivision surface of domain $\overline{\Omega}$ and boundary $\overline{\Gamma} = \partial\overline{\Omega}$. The shell deforms under the action of applied loads and adopts a deformed configuration characterized by a surface of domain Ω and boundary $\Gamma = \partial\Omega$. The position vectors $\overline{\boldsymbol{r}}$ and $\boldsymbol{r}$ of a material point in the reference and deformed configurations of the shell may be parameterized in terms of a system of curvilinear coordinates $\{\theta^1, \theta^2, \theta^3\}$ as:

$$\overline{\boldsymbol{r}}(\theta^1,\theta^2,\theta^3) = \overline{\boldsymbol{x}}(\theta^1,\theta^2) + \theta^3 \overline{\boldsymbol{a}}_3(\theta^1,\theta^2), \quad -\frac{h}{2} \le \theta^3 \le \frac{h}{2}$$

and

$$\boldsymbol{r}(\theta^1,\theta^2,\theta^3) = \boldsymbol{x}(\theta^1,\theta^2) + \theta^3 \boldsymbol{a}_3(\theta^1,\theta^2), \quad -\frac{h}{2} \le \theta^3 \le \frac{h}{2}$$

The functions $\overline{\boldsymbol{x}}(\theta^1,\theta^2)$ and $\boldsymbol{x}(\theta^1,\theta^2)$ furnish a parametric representation of the middle surface of the shell in the reference and deformed configurations, respectively (Fig. 6). The corresponding surface basis vectors are:

$$\overline{\boldsymbol{a}}_\alpha = \overline{\boldsymbol{x}}_{,\alpha} \quad \text{and} \quad \boldsymbol{a}_\alpha = \boldsymbol{x}_{,\alpha}$$

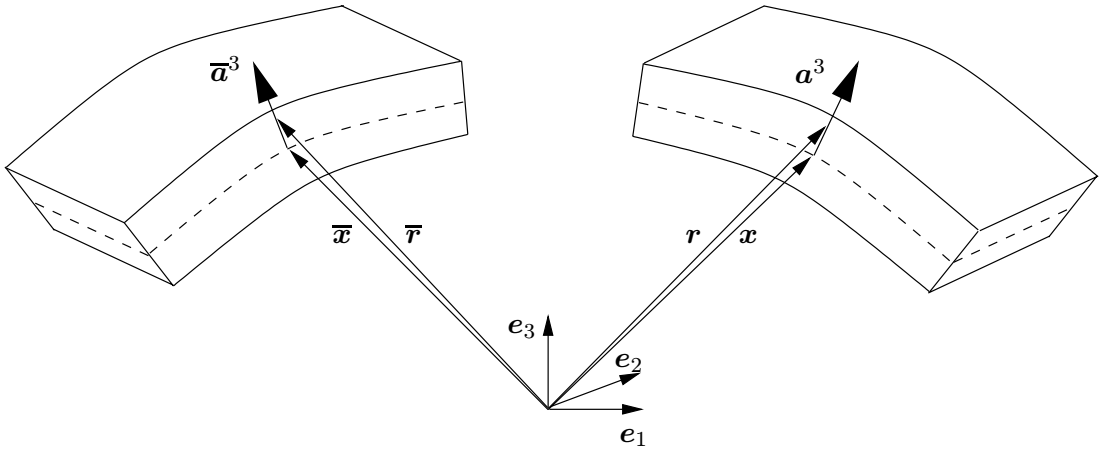

Figure 6: Shell geometry in the reference and the deformed configurations.

where the comma is used to denote partial differentiation with respect to θ^1 and θ^2 and the Greek indices take the value 1 and 2. The shell directors $\overline{\boldsymbol{a}}_3$ and $\boldsymbol{a}_3$ are defined as:

$$\overline{\boldsymbol{a}}_3 = \frac{\overline{\boldsymbol{a}}_1 \times \overline{\boldsymbol{a}}_2}{\sqrt{\overline{a}}} \quad \text{and} \quad \boldsymbol{a}_3 = \frac{\boldsymbol{a}_1 \times \boldsymbol{a}_2}{\sqrt{a}}$$

with the Jacobians of the surface coordinates:

$$\sqrt{\overline{a}} = |\overline{\boldsymbol{a}}_1 \times \overline{\boldsymbol{a}}_2| \quad \text{and} \quad \sqrt{a} = |\boldsymbol{a}_1 \times \boldsymbol{a}_2|$$

The covariant components of the surface metric tensors in turn follow as:

$$\overline{a}_{\alpha\beta} = \overline{\boldsymbol{a}}_\alpha \cdot \overline{\boldsymbol{a}}_\beta \quad \text{and} \quad a_{\alpha\beta} = \boldsymbol{a}_\alpha \cdot \boldsymbol{a}_\beta$$

whereas the covariant components of the curvature tensors are given by:

$$\overline{\kappa}_{\alpha\beta} = -\overline{\boldsymbol{a}}_{\alpha,\beta} \cdot \overline{\boldsymbol{a}}_3 \quad \text{and} \quad \kappa_{\alpha\beta} = -\boldsymbol{a}_{\alpha,\beta} \cdot \boldsymbol{a}_3$$

We define the following two strain measures for describing the change in the geometry between reference and the deformed geometry:

$$\alpha_{\alpha\beta} = \frac{1}{2}(\overline{a}_{\alpha\beta} - a_{\alpha\beta}) \quad \text{and} \quad \beta_{\alpha\beta} = \kappa_{\alpha\beta} - \overline{\kappa}_{\alpha\beta}$$

In particular, the in-plane components $\alpha_{\alpha\beta}$, or membrane strains, measure the straining of the surface and the components $\beta_{\alpha\beta}$, or bending strains, measure the bending or change in curvature of the shell, respectively. The linearized strain measures follow from:

$$\frac{d\alpha_{\alpha\beta}(\overline{\boldsymbol{x}} + \epsilon\boldsymbol{u})}{d\epsilon}|_{\epsilon=0} \quad \text{and} \quad \frac{d\beta_{\alpha\beta}(\overline{\boldsymbol{x}} + \epsilon\boldsymbol{u})}{d\epsilon}|_{\epsilon=0}$$

where $\boldsymbol{u}(\theta^1, \theta^2)$ is the displacement field of the middle surface of the shell. The membrane and bending strains are, therefore, of the form:

$$\alpha_{\alpha\beta} = \frac{1}{2}(\overline{\boldsymbol{a}}_\alpha \cdot \boldsymbol{u}_{,\beta} + \boldsymbol{u}_{,\alpha} \cdot \overline{\boldsymbol{a}}_\beta) \tag{3}$$

and

$$\beta_{\alpha\beta} = -\boldsymbol{u}_{,\alpha\beta}\cdot\overline{\boldsymbol{a}}_3 + \frac{1}{\sqrt{\overline{a}}}\left[\boldsymbol{u}_{,1}\cdot(\overline{\boldsymbol{a}}_{\alpha,\beta}\times\overline{\boldsymbol{a}}_2) + \boldsymbol{u}_{,2}\cdot(\overline{\boldsymbol{a}}_1\times\overline{\boldsymbol{a}}_{\alpha,\beta})\right] + \frac{\overline{\boldsymbol{a}}_3\cdot\overline{\boldsymbol{a}}_{\alpha,\beta}}{\sqrt{\overline{a}}}\left[\boldsymbol{u}_{,1}\cdot(\overline{\boldsymbol{a}}_2\times\overline{\boldsymbol{a}}_3) + \boldsymbol{u}_{,2}\cdot(\overline{\boldsymbol{a}}_3\times\overline{\boldsymbol{a}}_1)\right] \tag{4}$$

It is clear from these expressions that the displacement field $\boldsymbol{u}$ of the middle surface furnishes a complete description of the deformation of the shell and may therefore be regarded as the primary unknown of the analysis.

3.3 Weak Form of Equilibrium and Discretization

For simplicity, we shall assume throughout that the shell is linearly elastic with a strain energy density per unit area of the form:

$$W(\boldsymbol{u}) = \frac{1}{2}\frac{Eh}{1-\nu^2}H^{\alpha\beta\gamma\delta}\alpha_{\alpha\beta}\alpha_{\gamma\delta} + \frac{1}{2}\frac{Eh^3}{12(1-\nu^2)}H^{\alpha\beta\gamma\delta}\beta_{\alpha\beta}\beta_{\gamma\delta} \tag{5}$$

whereby the Einstein summation convention applies, ν denotes Poisson's ratio and E denotes Young's modulus. The fourth order constitutive tensor $H^{\alpha\beta\gamma\delta}$ is given by:

$$H^{\alpha\beta\gamma\delta} = \nu\,\overline{a}^{\alpha\beta}\overline{a}^{\gamma\delta} + \frac{1}{2}(1-\nu)\left(\overline{a}^{\alpha\gamma}\overline{a}^{\beta\delta} + \overline{a}^{\alpha\delta}\overline{a}^{\beta\gamma}\right) \tag{6}$$

In (eq. 5), the first term is the membrane strain energy density and the second term is the bending strain energy density. The shell is subject to a system of external dead loads consisting of distributed loads $\boldsymbol{q}$ per unit area of $\overline{\Omega}$, and axial forces $\boldsymbol{N}$ per unit length of $\overline{\Gamma}$. Under these conditions the potential energy of the shell takes the form:

$$\Phi[\boldsymbol{u}] = \int_\Omega W(\boldsymbol{u})\,d\Omega - \int_\Omega \boldsymbol{q}\cdot\boldsymbol{u}\,d\Omega - \int_\Gamma \boldsymbol{N}\cdot\boldsymbol{u}\,ds$$

The stable equilibrium configurations of the shell now follow from the principle of minimum potential energy:

$$\Phi[\boldsymbol{u}] = \inf_{\boldsymbol{v}\in V}\Phi[\boldsymbol{v}] \tag{7}$$

where V is the space of solutions consisting of all trial displacement fields $\boldsymbol{v}$ with finite energy $\Phi[\boldsymbol{v}]$. The Euler-Lagrange equations corresponding to the minimum principle (eq. 7) may be expressed in weak form as:

$$\langle D\Phi[\boldsymbol{u}],\boldsymbol{v}\rangle = \langle D\Phi^{\mathrm{i}}[\boldsymbol{u}],\boldsymbol{v}\rangle + \langle D\Phi^{\mathrm{e}}[\boldsymbol{u}],\boldsymbol{v}\rangle = 0 \tag{8}$$

In particular, the term internal energy has the form:

$$\langle D\Phi^{\mathrm{i}}[\boldsymbol{u}],\boldsymbol{v}\rangle = \int_\Omega \left[\frac{Eh}{1-\nu^2}H^{\alpha\beta\gamma\delta}\alpha_{\alpha\beta}(\boldsymbol{u})\alpha_{\gamma\delta}(\boldsymbol{v}) + \frac{Eh^3}{12(1-\nu^2)}H^{\alpha\beta\gamma\delta}\beta_{\alpha\beta}(\boldsymbol{u})\beta_{\gamma\delta}(\boldsymbol{v})\right]d\Omega$$

It is clear that the displacements and the trial functions must necessarily have square integrable first and second derivatives. Under suitable technical restrictions on the domain Ω and the applied loads, it therefore follows that V may be identified with the Sobolev space of functions $H^2(\Omega, R^3)$. In particular, an acceptable finite-element interpolation method must guarantee that all trial finite-element interpolants belong to this

space. Next we proceed to partition the domain Ω of the shell into a set of disjoint elements as induced by the original control mesh. The collection of element domains in the mesh is $\{\Omega_j,\ j = 1,\dots,n\}$, where Ω_j denotes the domain of element j and n is the total number of elements in the domain. The subdivision control mesh may be taken as a basis for introducing the interpolations of the general form:

$$\overline{\boldsymbol{x}}_h(\theta^1,\theta^2) = \sum_{l=1}^{L} N^l(\theta^1,\theta^2)\overline{\boldsymbol{x}}_l \quad \text{and} \quad \boldsymbol{u}_h(\theta^1,\theta^2) = \sum_{l=1}^{L} N^l(\theta^1,\theta^2)\boldsymbol{u}_l \tag{9}$$

where $\{N^l,\ l = 1,\dots,L\}$ are the shape functions, $\{\overline{\boldsymbol{x}}_l,\ l = 1,\dots,L\}$ are the coordinates of the control points in the reference configuration, $\{\boldsymbol{u}_l,\ l = 1,\dots,L\}$ are the corresponding nodal displacements, and L is the number of nodes in the mesh. Furthermore, an application of (eqs. 3 and 4) to the displacement interpolation (eq. 9) gives the finite-element membrane and bending strains in the form:

$$\boldsymbol{\alpha}_h(\theta^1,\theta^2) = \sum_{l=1}^{L} \boldsymbol{M}^l(\theta^1,\theta^2)\boldsymbol{u}_l \quad \text{and} \quad \boldsymbol{\beta}_h(\theta^1,\theta^2) = \sum_{l=1}^{L} \boldsymbol{B}^l(\theta^1,\theta^2)\boldsymbol{u}_l \tag{10}$$

The exact form of the matrices $\boldsymbol{M}^l$ and $\boldsymbol{B}^l$ can be found in [10]. Introducing the strain interpolations (eq. 10) into the weak form (eq. 8) and subsequent numerical integration of the integrals leads to the discrete equilibrium equation:

$$\boldsymbol{K}_h\boldsymbol{u}_h = \boldsymbol{f}_h \tag{11}$$

where $\boldsymbol{K}_h$ is the stiffness matrix and $\boldsymbol{f}_h$ is a force vector.

3.3.1 Remarks

- Theoretical considerations and numerical tests show that a one-point quadrature rule leads to a discrete stiffness matrix with full rank, and optimal convergence of the method. The integration point is at the barycenter of the elements. Sufficient conditions for the quadrature rule to preserve the order of convergence of the finite-element method may be found in [45].
- The derived strain-displacement relations (eqs. 10) and the introduced material model (eq. 6) are linear. The presented theory can thus only be applied in the small displacement and strain regime.
- The extension of the methods to the large deformation case can be found in [9].
- The resulting algebraic equation system (eq. 11) is, as usual for finite-element methods, sparse. We solve it with a standard direct method specially tailored for sparse matrices.
- A classical approach to avoid the use of smooth shape functions in finite-element computations is based on the theory of thick-shells with shear deformation [1, 4, 7, 40, 41]. The related finite-element implementations require only piecewise continuous shape functions, but lead to problems such as shear locking for thin-shells – especially in the presence of severe element distortion.

4 Design Space Exploration and Multi-Attribute Decision-Making

Engineering design requires a range of analysis methods, such as the subdivision method for thin-shell structural analysis described above, in order to assess one or more aspects of performance for any particular design candidate. However, several additional elements must also be available to the design engineer to make effective use of such analysis methods. The designer needs:

- some approach to determine or propose which candidates to analyze,
- some method for trading-off cost and fidelity of analysis, and
- a method for trading-off (or aggregating) multiple (usually competing) aspects of performance (*i.e.*, mass and stiffness).

The subdivision method for thin-shell structural analysis described above provides a powerful technique for trading-off cost and fidelity of analysis, by:

- permitting the use of a coarse mesh early in the design procedure when a large number of design alternatives are being considered, and the resources that can be applied to the (preliminary) analysis of any one alternative are small, and
- increasing the fidelity of the analysis, by subdivision refinement of the mesh, as the design process proceeds and the number of design alternatives being considered is reduced, and the resources that can be applied to the analysis of any one alternative grow.

This is particularly beneficial, because the underlying model of the shell does not need to be recreated as the design proceeds, only the degree of subdivision applied to the original model needs to be increased.

The multi-attribute character of engineering design makes it more than a simple optimization problem. In multi-attribute problems, trade-offs among criteria can play a determining role, and the designer is frequently interested in a Pareto frontier of points [18, 26, 46] rather than a single optimum.

A *Pareto point* is a point in the set of possible designs that matches or exceeds the performance of any other possible design point on at least one attribute; if one point is better than a second on all attributes, the second point is *dominated* and cannot be a Pareto point. The Pareto frontier is the set of Pareto points. A set of Pareto points comprising a Pareto frontier in a 2-dimensional problem is shown in Figure 7.

The choice of a trade-off strategy (or aggregation) determines which of the undominated (Pareto) points is selected as best satisfying the multiple criteria. Choosing an appropriate trade-off strategy is a crucial part of the engineering design process, principally because it can dramatically affect the result [31]. A family of functions, appropriate for engineering design, to perform this aggregation is introduced in [39].

It can be highly beneficial for the engineer to consider *sets* of designs [3]. As the design process proceeds, the size of the set of designs under consideration is reduced, as the fidelity of the analysis is increased. Set-based methods have been shown to facilitate design concurrency [47].

The design engineer's task involves proposing alternative solutions, coupled with an iterative exploration of the design space. The dimension of a typical design space may be in the tens or hundreds. Unless the measure of performance is an analytic function of the design variables (an unusual case), the engineer must construct the performance function through pointwise evaluation of the design space. Even for rapid performance calculations, "exhaustive" exploration of a design space (even to a modest resolution in each dimension) is prohibitively expensive; for calculations such as finite-element analysis that may take many minutes of cpu time, even a rudimentary exploration of the design space becomes impossible.

Methods for coping with this computational difficulty at any one level of design resolution include polynomial and other approximations of the performance function (Design of Experiments [28, 33, 37], Kriging [42], MARS [15], Response Surface methods [21]), local approximation of partial derivatives (sensitivity analysis [22]), directed pointwise search (classical optimization [32]) and *ad hoc* selection guided by experience and intuition.

For multi-attribute problems, decision analysis methods are used to assess the performance of *sets* of designs (the Method of Imprecision [3, 49]), and to trade-off multiple competing aspects of the design (utility theory [18], matrix methods [34], and aggregation methods [31, 39]).

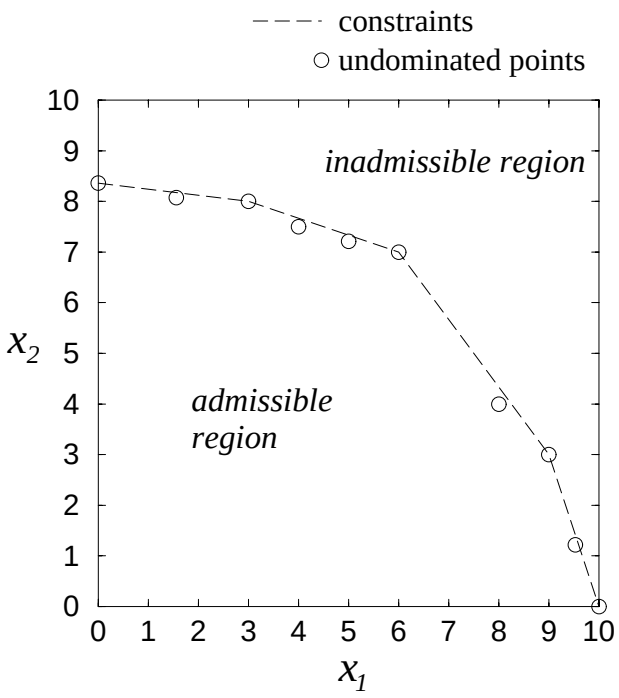

Figure 7: A Set of Pareto Points.

Finally, engineers routinely use models of differing resolution at different stages of a design process, for example, progressing from linear beam calculations at an early stage of design to a finely-meshed non-linear finite-element analysis when the geometry of the part is more precisely described. Such models cannot be described as *multi-resolution*, however, for the engineer must employ different models to change resolutions.

The subdivision method for thin-shell structural analysis described above provides a true, natural, multi-resolution analysis, where one model supports many different resolutions. As with other modeling methods, increased fidelity comes at an increased computational cost. However, here the designer specifies a single parameter (the level of subdivision) to choose faster analyses in the early stages and more accurate ones later, rather than building a new model for each desired level of resolution of the same design.

5 Examples

We present two design examples to illustrate the framework presented above for integrated modeling, finite-element analysis and design of thin-shells based on subdivision surfaces. In the examples, the initial design is improved with respect to multiple objective functions. For optimization we employ a simple pattern search algorithm. The search is based only on the value of the objective function and does not require function derivatives. If derivatives (sensitivities) are available more sophisticated optimization algorithms can be utilized (see, *e.g.*, [13, 30] among many others).

5.1 Square Plate

The first example is the design of a uniformly loaded roof over a square shaped area (Figure 8). The roof is supported at the four corners. The design objective is to maximize the stiffness (or to minimize the

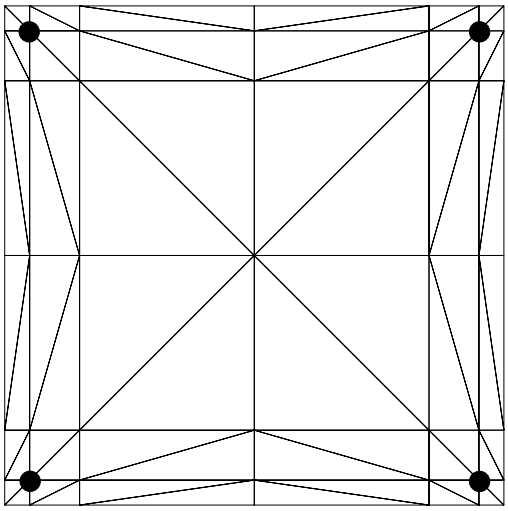

Figure 8: Definition of the plate test problem and a typical mesh used in the calculations.

compliance) of the structure which can be expressed more formally as:

$$\min_{\boldsymbol{s}} \quad \boldsymbol{u}^T \boldsymbol{K} \boldsymbol{u} \tag{12}$$

where $\boldsymbol{s}$ is the set of design variables, $\boldsymbol{u}$ are the displacements, and $\boldsymbol{K}$ is the stiffness matrix. Although, not explicitly indicated in (eq. 12), the stiffness matrix and the displacements depend on the design variables. Furthermore, the range of the design variables $\boldsymbol{s}$ is given by the user. Within the subdivision framework the vertices of the control mesh are the design variables. For the plate example we chose as design variables the out of plane components of the control vertices in Figure 8. In order to compute the stiffness in (eq. 12) during the design space exploration we utilize the finite-element method based on the subdivision shape functions as described earlier. However, the resolution of the control mesh is not sufficient for finite-element analysis. The control mesh is subdivided twice prior to the computation (Figure 9, left). Using the finite-element mesh vertices directly as design variables would lead to too many unknowns during the optimization procedure. In addition it leads to oscillations in the optimized shape so that the results of the optimization are useless [13]. Consequently the parameters of the CAD model are chosen as the optimization variables. In a traditional framework this requires the generation of a finite-element mesh separate from the original CAD model, bringing with it the computational disadvantage of keeping two representations [6, 16, 30]. The subdivision based approach is computationally efficient and representationally unified way to use the subdivision control mesh to parameterize both the geometry and the finite-element model.

The optimized roof structure is shown in Figure 9. For thin-shells the response to membrane strain is much stiffer than to bending strain. Accordingly, the stiffness of the initial flat plate with bending energy only, can be increased by changing the initial geometry of the shell as shown in Figure 9. Note the small features close to the free boundaries of the optimized shape. Through the optimization process the objective function in (eq. 12) could be minimized from 22541.32 to 55.39. This improvement demonstrates the well known strong influence of the curvature on stiffness.

5.2 VW Hood

As an illustration of the value of the multiresolution simulation method using subdivision surfaces, consider the *circa*-1960 VW Beetle hood shown in Figure 10. The engineering design problem for the VW hood is to select a geometry of the hood to obtain superior performance in a number of aspects of performance, both

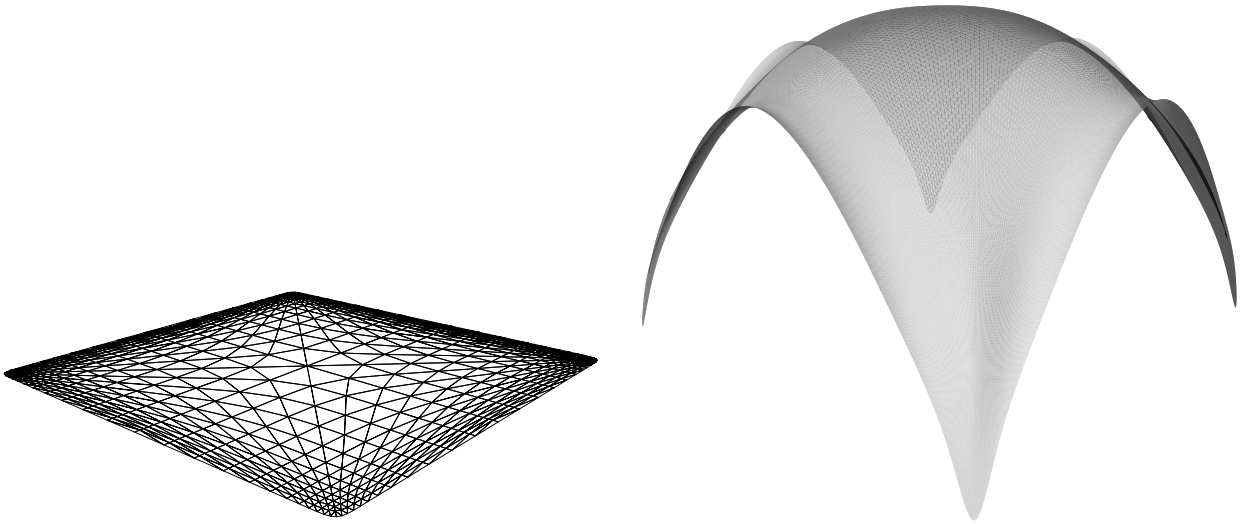

Finite-element mesh Optimum shape

Figure 9: Square Plate Example.

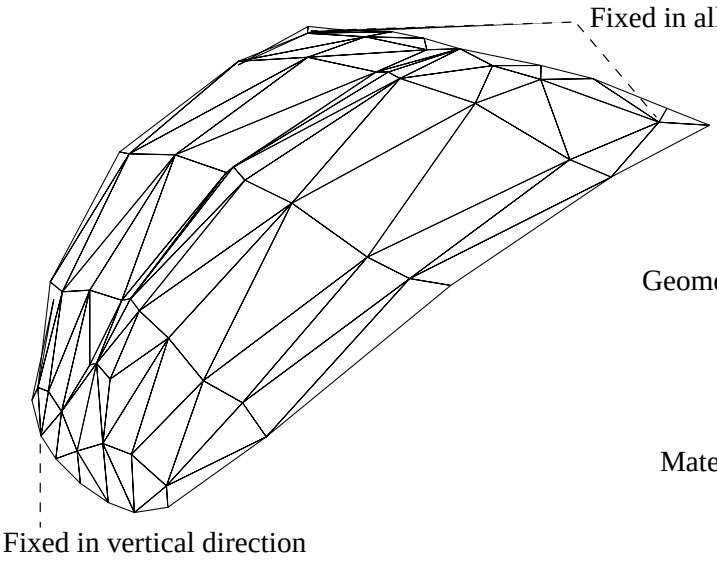

Geometry : $\max x - \min x = 40.79$
$\max y - \min y = 42.03$
$\max z - \min z = 26.36$
$h = 0.12$

Material : $E = 12500$
$\nu = 0.290$
$\rho = 0.1$

Figure 10: Definition of the hood problem.

measured and unmeasured. Chief among these performance concerns is a measure of torsional stiffness (the hood should not deform unacceptably if lifted from a point off-center at the front), which will be computed using the finite-element method on the subdivision surface described above. In addition, the total weight and the storage volume under the hood are calculated, and the styling, manufacturability, and usability of the hood are taken into account.

The original surface model (Figure 10) has 63 control points. There are 28 reflected pairs, leaving 35 unique control points if symmetry is enforced. Of those 35 points, 12 lie on the edge of the hood, and as the hood boundary is presumed to be fixed, those 12 points are fixed as well. It would be possible to treat the 23 remaining control points as design variables, and vary them individually. In order to lessen deviations from the original styling (the hoods that we consider ought to look like a VW), these 23 control points are varied using four non-dimensional geometric parameters: the swell of the hood (Figure 11, left), the depth

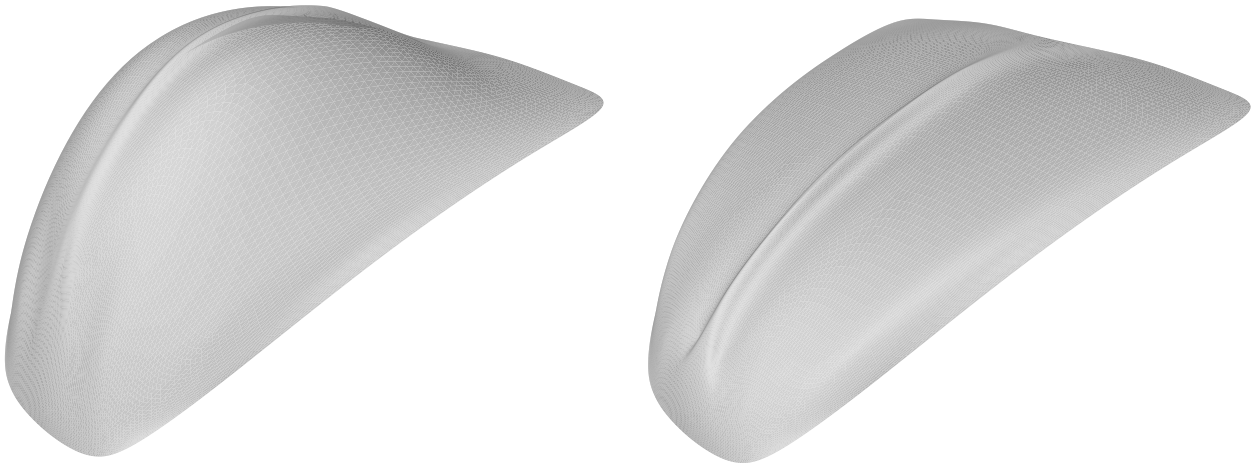

Center swell Crease

Figure 11: VW Hood Variations.

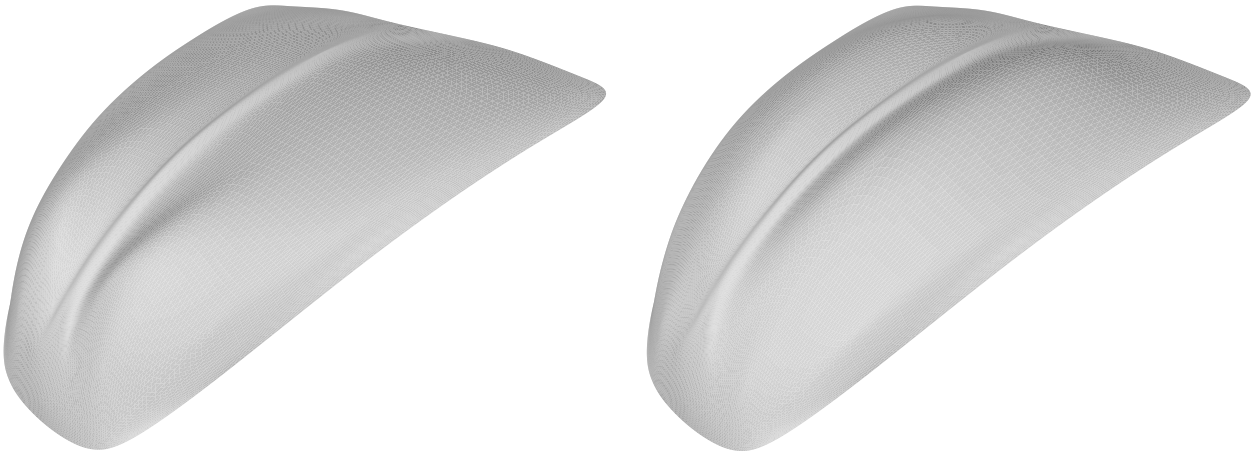

Lower side swell Upper side swell

Figure 12: VW Hood Variations.

of the characteristic center crease (Figure 11, right), the swell of the upper portion of each side of the hood (Figure 12, right), and the swell of the lower portion of each side of the hood (Figure 12, left). At the reference configuration all design variables have a value of one, and at zero all curves flatten to straight lines.

As mentioned above, the design problem for the VW hood is not one of simple optimization. Since the finite-element mesh is easily modified, it is possible to "optimize" the design variables for minimum weight (Figure 13), or maximum stiffness (Figure 13). These "optima" may be undesirable for other reasons such as styling or manufacturability; also, one may sacrifice too much stiffness to achieve the lightest possible design, or vice versa. Using the lowest resolution finite-element analysis and an iterative search process, an approximate Pareto frontier on trade-offs between weight and stiffness can be found. As shown in Figure 14, there are many Pareto points, many of which significantly outperform the reference configuration in both weight and stiffness. Acquisition of the approximate Pareto frontier is made possible by use of the fastest

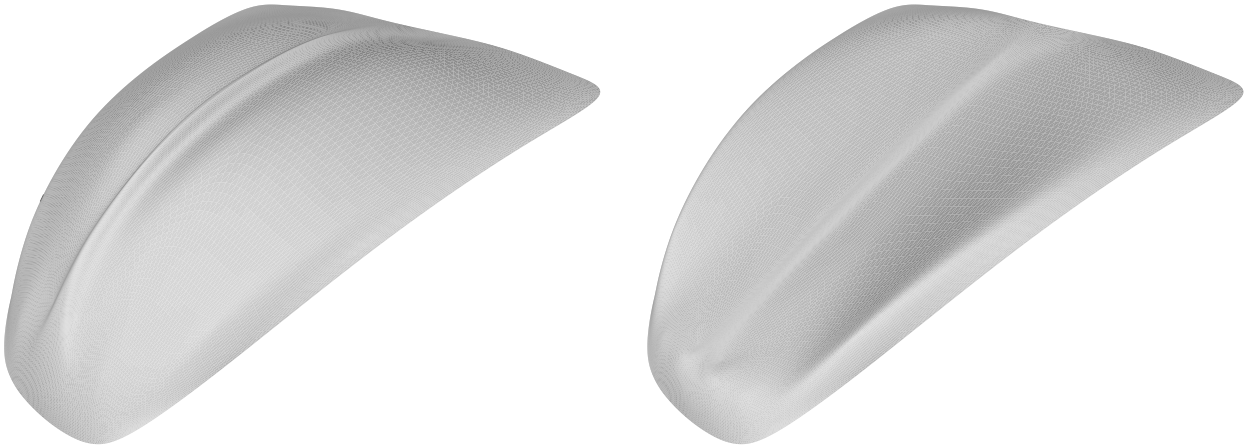

Optimized with respect to weight Optimized with respect to stiffness

Figure 13: Optimized VW hood.

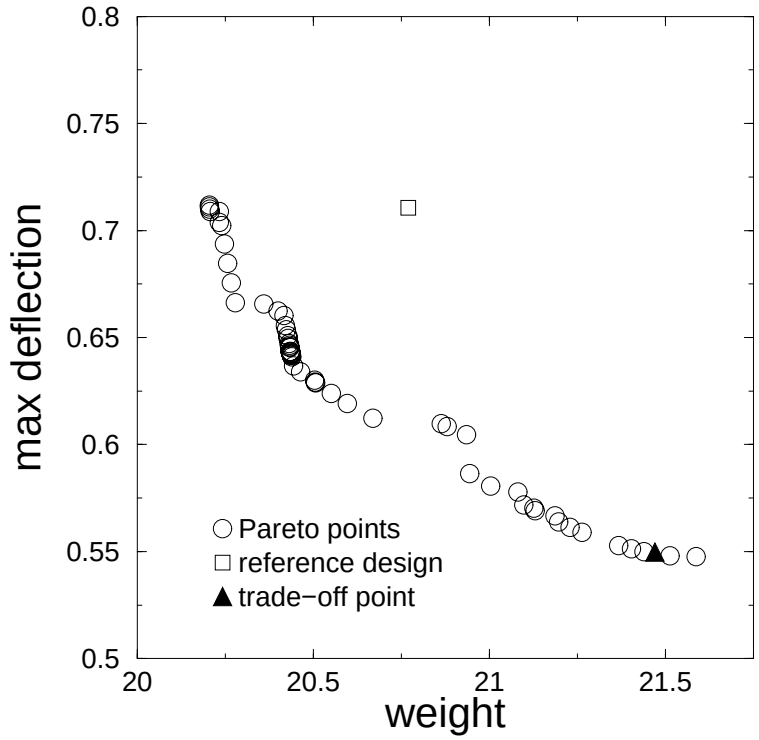

Figure 14: VW Pareto frontier

Figure 15: VW hood: Trade-off.

(coarsest) analysis; when a smaller region of design space is explored at the next design iteration, a finer, more accurate finite-element analysis can be employed.

The search for desirable designs can be further hastened by the use of approximations (which were not used in this example), and by *a priori* analysis of the trade-off between performance measures. By determining trade-off strategies and weights as described in [38], it is possible to search directly for a solution to fulfill a desired level of trade-off and relative importance weighting among the attributes. One such solution, representing a relatively non-compensating trade-off ($s = -10$), is shown in Figure 15, which appears as a black triangle in Figure 14. This particular solution is relatively insensitive to deviations from equal importance weights for the two attributes, and does not differ much from the minimum weight solution. As was shown in [38], every point on the Pareto frontier is the optimum for some trade-off strategy and pair of weights, so different decision analysis could lead to different solutions. In any case, the amount of necessary computation is greatly reduced by choosing importance weighting and a degree of compensation between attributes in advance [38].

6 Summary and Conclusions

We have proposed subdivision surfaces as a common foundation for modeling, simulation, and design in a unified framework. Subdivision surfaces provide a flexible and efficient tool for arbitrary topology free-form surface modeling, avoiding many of the problems inherent in traditional spline patch based approaches. In addition, the underlying basis functions are ideally suited to the finite-element analysis of thin-shells. The resulting solvers are highly scalable, providing an efficient computational foundation for design exploration and optimization. In particular, the ability to represent smooth surfaces with a relatively coarse control mesh greatly facilitates geometrical optimization.

Many engineering design applications require geometric modeling and mechanical simulation of thin flexible structures, such as those found in the automotive and aerospace industries. Traditionally, geometric modeling, mechanical simulation, and engineering design are treated as separate modules requiring different methods and representations. Due to this representational incompatibility, the transition from geometric

modeling to mechanical simulation, and *vice versa*, requires substantial effort. A straightforward transition between the different representations is particularly important for engineering design purposes. Subdivision surfaces provide a new formalism for overcoming these difficulties and effecting a seamless integration of modeling, finite-element analysis, and design of thin-shell structures. The examples of application presented here illustrate the versatility and effectiveness of this paradigm.

Acknowledgements

Special thanks to Leif Kobbelt, Max-Planck-Institut für Informatik, Saarbrücken, who modeled the VW Beetle hood. The support of DARPA and NSF through Caltech's OPAAL Project (DMS-9875042) is gratefully acknowledged. Additional support was provided by NSF under grant numbers: ACI-9624957, ACI-9721349, ASC-8920219, DMI-9523232, DMI-9813121, through a Packard fellowship to PS, and by Alias|Wavefront. Any opinions, findings, conclusions, or recommendations expressed in this publication are those of the authors and do not necessarily reflect the views of the sponsors.

References

[1] AHMAD, S., IRONS, B., AND ZIENKIEWICZ, O. Analysis of Thick and Thin Shell Structures by Curved Finite Elements. *Internat. J. Numer. Methods Engrg. 2* (1970), 419–451.

[2] ALIAS|WAVEFRONT. *Maya, 2.5*. Toronto.

[3] ANTONSSON, E. K., AND OTTO, K. N. Imprecision in Engineering Design. *ASME Journal of Mechanical Design 117(B) (Special Combined Issue of the Transactions of the ASME commemorating the 50th anniversary of the Design Engineering Division of the ASME.)* (June 1995), 25–32. Invited paper.

[4] BELYTSCHKO, T., STOLARSKI, H., LIU, W., CARPENTER, N., AND ONG, J. Stress Projection for Membrane and Shear Locking in Shell Finite-Elements. *Comput. Methods Appl. Mech. Engrg. 51* (1985), 221–258.

[5] BIERMANN, H., LEVIN, A., AND ZORIN, D. Smooth Subdivision Surfaces with Normal Control. Courant Institute of Mathematical Sciences, New York, Preprint, 1999.

[6] BLETZINGER, K., AND RAMM, E. Form Finding of Shells by Structural Optimization. *Engng. Comput.* (9 1993), 27–35.

[7] BÜCHTER, N., RAMM, E., AND ROEHL, D. 3-Dimensional Extension of Nonlinear Shell Formulation Based on the Enhanced Assumed Strain Concept. *Internat. J. Numer. Methods Engrg. 37* (1994), 2551–2568.

[8] CATMULL, E., AND CLARK, J. Recursively Generated B-Spline Surfaces on Arbitrary Topological Meshes. *Comput. Aided Design 10*, 6 (1978), 350–355.

[9] CIRAK, F., AND ORTIZ, M. Fully C^1-Conforming Subdivision Elements for Finite Deformation Thin-Shell Analysis. *Submitted, Internat. J. Numer. Methods Engrg.* (2000).

[10] CIRAK, F., ORTIZ, M., AND SCHRÖDER, P. Subdivision Surfaces: A New Paradigm for Thin-Shell Finite-Element Analysis. *In print, Internat. J. Numer. Methods Engrg. 47* (2000).

[11] DOO, D., AND SABIN, M. Behaviour of Recursive Division Surfaces Near Extraordinary Points. *Comput. Aided Design 10*, 6 (1978), 356–360.

[12] DYN, N., LEVIN, D., AND GREGORY, J. A Butterfly Subdivision Scheme for Surface Interpolation with Tension Control. *ACM Trans. Graphics 9*, 2 (1990), 160–169.

[13] HAFTKA, R., AND GRANDHI, R. Structural Shape Optimization - A Survey. *Comput. Methods Appl. Mech. Engrg. 57* (1986), 91–106.

[14] HALSTEAD, M., KAAS, M., AND DEROSE, T. Efficient, Fair Interpolation using Catmull-Clark Surfaces. In *Computer Graphics (SIGGRAPH '93 Proceedings)*, 1993.

[15] HSIEH, C., AND OH, K. MARS: A computer-based method for achieving robust systems. In *The Integration of Design and Manufacture, Volume I*, 115–120, June 1992.

[16] IMAM, M. Three-dimensional shape optimization. *Internat. J. Numer. Methods Engrg. 18* (1982), 661–673.

[17] KAGAN, P., FISCHER, A., AND BAR-YOSEPH, P. Integrated Mechanically Based CAE System. In *Proceedings of Fifth Symposium on Solid Modeling and Applications*, W. Bronsvoort and D. Anderson, Eds., 23–30, June 1999.

[18] KEENEY, R., AND RAIFFA, H. *Decisions with Multiple Objectives: Preferences and Value Tradeoffs*. Cambridge University Press, Cambridge, U.K., 1993.

[19] KHODAKOVSKY, A., AND SCHRÖDER, P. Fine Level Feature Editing for Subdivision Surfaces. In *Proceedings of Fifth Symposium on Solid Modeling and Applications*, W. Bronsvoort and D. Anderson, Eds., 203–211, June 1999.

[20] KOBBELT, L., HESSE, T., PRAUTZSCH, H., AND SCHWEIZERHOF, K. Iterative Mesh Generation for FE-Computations on Free Form Surfaces. *Engng. Comput. 14* (1997), 806–820.

[21] KORNGOLD, J. C., AND GABRIELE, G. A. Multidisciplinary Analysis and Optimization of Discrete Problems Using Response Surface Methods. In *Advances in Design Automation - 1995*, vol. DE-82, 173–180, Sept. 1995.

[22] LANGNER, W. J. Sensitivity Analysis and Optimization of Mechanical System Design. In *Advances in Design Automation - 1988*, S. S. Rao, Ed., vol. DE-14, 175–182, Sept. 1988.

[23] LEVIN, A. A Combined Subdivision Scheme Based on Catmull Clark's Scheme. Tech. rep., School of Mathematical Sciences, Tel-Aviv University, 1998.

[24] LEVIN, A. Combined Subdivision Schemes for the Design of Surfaces Satisfying Boundary Conditions. *Computer Aided Geometric Design 16* (1999), 345–354.

[25] LOOP, C. Smooth Subdivision Surfaces Based on Triangles. Master's thesis, University of Utah, Department of Mathematics, 1987.

[26] LUCE, R., AND RAIFFA, H. *Games and Decisions*. J. Wiley and Sons, New York, 1957. Dover Edition, 1985.

[27] MANDAL, C., QIN, H., AND VEMURI, B. A Novel FEM-Based Dynamic Framework for Subdivision Surfaces. In *Proceedings of Fifth Symposium on Solid Modeling and Applications*, W. Bronsvoort and D. Anderson, Eds., 191–202, June 1999.

[28] MONTGOMERY, D. C. *Design and Analysis of Experiments*. J. Wiley and Sons, New York, NY, 1991.

[29] NAGHDI, P. *Handbuch der Physik, Mechanics of Solids II*, vol. VI a/2. Springer, Berlin, 1972, ch. The theory of shells.

[30] OLHOFF, N., BENDSOE, M., AND RASMUSSEN, J. On CAD-Integrated Structural Topology and Design Optimization. *Comput. Methods Appl. Mech. Engrg. 89* (1991), 259–279.

[31] OTTO, K. N., AND ANTONSSON, E. K. Trade-Off Strategies in Engineering Design. *Research in Engineering Design 3*, 2 (1991), 87–104.

[32] PAPALAMBROS, P., AND WILDE, D. *Principles of Optimal Design*. Cambridge University Press, Cambridge, U.K., 1988.

[33] PHADKE, M. *Quality Engineering Using Robust Design*. Prentice Hall, Englewood Cliffs, NJ, 1989.

[34] PUGH, S. *Total Design*. Addison-Wesley, New York, NY, 1990.

[35] REIF, U. A Unified Approach to Subdivision Algorithms Near Extraordinary Vertices. *Comput. Aided Geom. Design 12*, 2 (1995), 153–174.

[36] REIF, U., AND SCHRÖDER, P. Curvature Smoothness of Subdivision Surfaces. Tech. Rep. TR-00-03, California Institute of Technology, 2000.

[37] SACKS, J., WELCH, W. J., MITCHELL, T. J., AND WYM, H. P. Design and Analysis of Computer Experiments. *Statistical Science 4*, 4 (Feb. 1989), 409–435.

[38] SCOTT, M. *Formalizing Negotiation in Engineering Design*. PhD thesis, California Institute of Technology, Pasadena, CA, June 1999.

[39] SCOTT, M. J., AND ANTONSSON, E. K. Aggregation Functions for Engineering Design Trade-offs. In *9th International Conference on Design Theory and Methodology*, vol. 2, 389–396, Sept. 1995.

[40] SIMO, J., AND FOX, D. On a Stress Resultant Geometrically Exact Shell Model. Part I: Formulation and Optimal Parameterization. *Comput. Methods Appl. Mech. Engrg. 72* (1989), 267–304.

[41] SIMO, J., FOX, D., AND RIFAI, M. On a Stress Resultant Geometrically Exact Shell Model. Part II: The Linear Theory; Computational Aspects. *Comput. Methods Appl. Mech. Engrg. 73* (1989), 53–92.

[42] SIMPSON, T. W., PEPLINSKI, J., KOCH, P. N., AND ALLEN, J. K. On the Use of Statistics in Design and the Implications for Deterministic Computer Experiments. In *9th International Conference on Design Theory and Methodology*, sep 1997.

[43] STAM, J. Fast Evaluation of Catmull-Clark Subdivision Surfaces at Arbitrary Parameter Values. In *Computer Graphics (SIGGRAPH '98 Proceedings)*, 1998.

[44] STAM, J. Fast Evaluation of Loop Triangular Subdivision Surfaces at Arbitrary Parameter Values. In *Computer Graphics (SIGGRAPH '98 Proceedings, CD-ROM supplement)*, 1998.

[45] STRANG, G., AND FIX, G. J. *An Analysis of the Finite Element Method*. Prentice-Hall, Englewood Cliffs, N.J., 1973.

[46] VON NEUMANN, J., AND MORGENSTERN, O. *Theory of Games and Economic Behavior*, 2nd ed. Princeton University Press, Princeton, NJ, 1953.

[47] WARD, A. C., LIKER, J. K., SOBEK, D. K., AND CRISTIANO, J. J. The Second Toyota Paradox: How Delaying Decisions Can Make Better Cars Faster. *Sloan Management Review 36*, 3 (Spring 1995), 43–61.

[48] WARREN, J. Subdivision Methods for Geometric Design. Unpublished manuscript, Department of Computer Science, Rice University, November 1995.

[49] WOOD, K. L., AND ANTONSSON, E. K. Computations with Imprecise Parameters in Engineering Design: Background and Theory. *ASME Journal of Mechanisms, Transmissions, and Automation in Design 111*, 4 (Dec. 1989), 616–625.

[50] ZIENKIEWICZ, O., AND TAYLOR, R. *The Finite Element Method - Volume 2*. McGraw-Hill Book Company, Berkshire, 1989.

[51] ZORIN, D. A Method for Analysis of C^1- Continuity of Subdivision Surfaces. *SIAM J. Num. Anal. submitted* (1998).

[52] ZORIN, D., AND SCHRÖDER, P., Eds. *Subdivision for Modeling and Animation* (1999), Computer Graphics (SIGGRAPH '99 Course Notes).

[53] ZORIN, D., SCHRÖDER, P., AND SWELDENS, W. Interpolating Subdivision for Meshes with Arbitrary Topology. In *Computer Graphics (SIGGRAPH '96 Proceedings)*, 1996.